

RESEARCH ARTICLE

A Hybrid Meta-heuristic Algorithm for Optimum Micro-robotic Position Control with PID Controller

Abdullah Baihan¹ · Ehab Ghith² · Harish Garg³ · Seyedali Mirjalili⁴ · Davut Izci^{5,8,9} · Mostafa Rashdan⁶ · Mohammad Salman⁶ · Kashif Saleem⁷

Received: 25 July 2024 / Revised: 14 February 2025 / Accepted: 12 March 2025

© The Author(s) 2025

Abstract

The present paper aims to propose a novel hybrid algorithm, where the Arithmetic Optimization Algorithm (AOA) and Rat Swarm Optimization (RSO) are employed for the proportional-integral-derivative (PID) controller to control the position of a micro-robotics system. In the algorithm proposed, we combine the exploratory mechanisms of AOA with RSO's exploitative behaviors. The proposed algorithm is employed for identifying the PID controller optimal parameters considering six different objective functions. Using CEC 2017 benchmark functions, the proposed hybrid is evaluated, and these functions' performance is compared with the existing multiple algorithms. The statistical results are compared with the AOA, Jellyfish Search Optimization, and Harries Hawk Optimization algorithm for identifying the optimal PID controller settings considering multiple fitness functions. We consider performance indicators like PID controller parameters, rise time, settling time, and fitness values. The fetched simulation results revealed that, among all investigated fitness functions, the developed controller based on HAOARSO is the most effective algorithm for delivering global optimal solutions with less settling time and rise time, enabling the implementation on such optimization issues. Finally, the validation via MATLAB/Simulink simulations underscores the efficacy of the proposed algorithm.

Keywords PID controller · Hybrid algorithm · Arithmetic optimization algorithm · Rat swarm optimization · Minimally invasive surgery

1 Introduction

Recent attention has been focused on magnetic micro-particles and nano-particles in the fields of nanotechnology and nanomedicine [1, 2]. The particles' small size enables accessing deep areas inside the human body, making them suitable for targeted therapy and various biomedical applications [3–8]. The use of biodegradable magnetic nanoparticles, nano capsules, and micro-particles (referred to as magnetic drug carriers) for drug delivery has been proposed by numerous researchers [9–13]. These carriers can be directed towards diseased cells by injecting them into the circulatory system and applying external magnetic fields. However, the positioning and control of such carriers in fluid flowing streams pose challenges due to their miniature size. This recurrent problem has the potential to affect targeted therapy and biomedical applications.

Recent studies have introduced self-driven [14–17] and magnetic mechanisms to address the issue of stream flow inside fluidic channels. These studies aim to prevent unwanted flow in the channels. One approach involves the use of self-propelled microjets, particularly open-loop control, which can overcome the propagation of



hydrogen peroxide solution within the channels [14]. The closed-loop control, linked to microscopic image guidance, enhances the microjets' control accuracy and enables solution in hydrogen peroxide streams [18]. These microjets possess the ability to control solution flow and perform various tasks. However, their application in biomedical contexts is limited due to the associated toxicity of their locomotion mechanism. Presently, no sufficient research is present on determining the optimal path for microjets to follow with minimal control effort and time. Nacev et al. [19] successfully achieved ferromagnetic nanoparticles positioning inside rats by external magnetic fields being directed without feedback. Employing fluids with various viscosities, Bekharet et al. [17] offered a predictive control method designed for magnetic microrobots present in microfluidic arterial bifurcations.

Furthermore, paramagnetic micro-particles' input control minimally in three-dimensional (3D) space was accomplished utilizing a closed configuration electromagnetic system [20]. In Jasper D. et al., paramagnetic micro-particles are successfully set up for a spherical site, achieving settling error at an 8.4 μm , with the system reaching control opposition [21]. With a 100 μm average diameter, these microparticles were employed in the experiment, with a hollow coil and water as the medium. Ramy et al. simulated a similar experiment using a solid coil and achieved an 8 μm settling error [22]. Ghith et al. achieved a 4 μm settling error with the same setup of experiment. When compared to earlier studies, it has been found that the Sparrow Search Algorithm (SSA) can decrease the settling error by up to 50% [23–30].

To realize the control objectives, the controller needs to be appropriately and sufficiently constructed. Despite the various control techniques that have been created, PID controller is still used because it is easily implementable, customizable, and simply structured. Nevertheless, until the PID control reaches its maximum efficiency, it is still challenging to adjust it correctly. Numerous designs have been put forth. Examples of these designs involve the PID controller and Ziegler and Nichols, its most well-known techniques. For instance, a popular approach is the integration of GA with PID controllers, where GA is employed for PID parameters to achieve optimal performance. Hence, traditional PID controllers are outperformed in various applications, such as industrial processes and robotic systems. Similarly, hybrid PSO-based control designs have been successfully applied to nonlinear systems, where the global search capability of PSO aids in finding optimal solutions which are difficult for traditional control techniques to achieve. Moreover, hybrid methods have been proposed to enhance adaptive control systems, particularly in uncertain or time-varying environments. These approaches leverage the strengths of both model-based control strategies and data-driven optimization algorithms, offering a balance between theoretical robustness and practical flexibility. For example, combining fuzzy logic controllers with optimization techniques such as simulated annealing or differential evolution has resulted in systems that can adapt to unforeseen changes in system dynamics [31–37].

To solve optimization problems, metaheuristics have been quite popular lately. In contrast, these methods are more adaptable and simpler to use, and they do not require gradient information. Two classes are included under metaheuristic techniques: single solution-based and population-based algorithms. As the trajectory or single-based optimization method names imply, only one solution is created and improve throughout the optimization process. In contrast, multiple solutions can be generated in the population-based algorithm. Another classification of metaheuristics leans on inspiration: Swarm intelligence, evolutionary-based, human-based and physics-based [38–42].

Hybrid algorithms, which combine the strengths of multiple optimization or control techniques, have gained significant attention in control system design due to their ability to solve complex, nonlinear, and high-dimensional problems. In control theory, where system behavior is often dynamic and influenced by various factors, hybrid algorithms offer a versatile approach to improving system performance, robustness, and stability. Combinations of classical methods, like Proportional-Integral-Derivative (PID) controllers, with optimization algorithms such as Ant Colony Optimization (ACO), Genetic Algorithms (GA), and Particle Swarm Optimization (PSO) have

been explored in recent research in hybrid control design. With an aim for controller parameters optimization in real-time, these hybrid systems improve adaptability to changes in system dynamics and disturbances.

A key advantage of hybrid algorithms in control design is their ability to address multiple objectives simultaneously—such as minimizing tracking error, maximizing stability, and reducing energy consumption—while offering more efficient and adaptable solutions. Hybrid control designs have been successfully applied in areas such as robotics, autonomous vehicles, power systems, and aerospace engineering, where systems are complex, highly dynamic, and require real-time adjustments. In light of these developments, the proposed hybrid algorithm-based approach in this paper offers potential for significant improvements in control system performance. With complementary strengths of various algorithms leveraged, the accuracy and efficiency of control designs can be enhanced by hybrid systems in ways that would be difficult to achieve with individual approaches alone. Some drawbacks of the single optimization strategy are fragile exploitation, possibly trapping in local optima, and an inappropriate balance between exploration and exploitation. It is crucial to remember that hybridizing two techniques could result in higher computing costs, especially for real-world engineering problems with high dimensions. To prevent the loss of exploration, an adaptive adjustment, during the optimization process, of constants in the hybrid version must be carried out. For the subsequent rounds, hybrid algorithms ought to prioritize enhancing the exploration of algorithms. Thus, a practical tactic to enhance algorithm performance while lowering computational cost is to combine two or more algorithms into a single component [43–48].

Rat swarm optimization (RSO) and hybrid arithmetic optimization algorithm (AOA) are proposed in this work. RSO and AOA are population-based optimization algorithms and were recently developed by Dhiman et al. [42] and Trojovský et al. [49], respectively. The RSO optimizer draws its primary inspiration from the pursuing and attacking activities of rats in their environment, while the AOA mimics the natural behavior of pelicans when hunting. The hybrid algorithm developed combines the exploitation advantages of AOA and the exploration advantages of RSO. This is achieved by executing them in parallel and choosing the current best-obtained solutions for the next iteration. Using CEC 2017 benchmark functions, the proposed HAOARSO optimizer is validated and compared with AOA and RSO. Then, we employ the developed HAOARSO algorithm for identifying the PID controller optimal parameters, considering six different objective functions that involve integral of square time multiplied by square error (ISTSE), integral square error (ISE), integral square time multiplied by error squared (ISTES), integral absolute error (IAE), integral of time multiplied by square error (ITSE), and integral of time multiplied by absolute error (ITAE). The present paper contributions are summarized below.

- (1) Developing a novel hybrid optimization named the HAOARSO algorithm, which incorporates the best features of rat swarm optimization and arithmetic optimization algorithm to control the position of the micro-robotics system optimally.
- (2) Employing CEC 2017 benchmark functions that comprise various types of unimodal, multimodal, and fixed-dimensional composite functions for measuring the effectiveness of the developed hybrid HAOARSO through different statistical analyses.
- (3) Designating the PID controller optimum parameters considering six dissimilar fitness functions, i.e., ITSE, ISE, IAE, ISTES, ISTSE, and ITAE, using HAOARSO, JSO, HHO, and AOA.
- (4) The proposed hybrid HAOARSO algorithm dominance and efficacy in identifying the optimal tuning of PID parameters to control the micro-robotics system position are confirmed in the results.

This paper is structured as follows: Sect. 2 offers an overview of the PID controller, the micro-robotic system model, optimization methods, and fitness function types. Section 3 presents the performance analysis for rat swarm optimization, and hybrid arithmetic optimization algorithm. In Sects. 4, 5, and 6, the simulation, discussion, and conclusions are presented, respectively.

2 Materials and Methods

2.1 Micro-robotic System Model

To design particles, a paramagnetic material is utilized, specifically iron oxide in lactic acid. 100 μm in diameter, these particles have two factors influencing their velocity. The viscous drag and magnetic forces are generated via the micro-particles and are dependent on the magnetic field produced by coils. Furthermore, the maximal velocity can be attained when acceleration equals zero, with balanced viscous drag and magnetic forces. The equation below is employed for defining magnetic force [23–31].

$$F = \nabla\alpha_p V_p B^2 \quad (1)$$

The given equation involves several variables. The particles volume is represented by V_p , and the magnetic flux density is denoted by B . The magnetic flux leans on distance and time, while α_p and V_p indicate constant values. The equation provided below illustrates the variables that are utilized to substitute V_p for force production:

$$F = \frac{4}{3}\pi\alpha_p r_p^3 \nabla B^2 \quad (2)$$

In the given equation, r_p represents the radius of micro-particles, and a representation of the drag force is given below in this equation.

$$F_d = -6\pi\eta r_p v \quad (3)$$

Viscosity, denoted by η , and the micro-particle velocity which v represents, are related in accordance with Newton's second law of motion.

$$\sum F = m_p a_p$$

$$\frac{4}{3}\pi\alpha_p r_p^3 \nabla B^2 - 6\pi\eta r_p v = m_p a_p$$

$$v = \frac{\frac{4}{3}\pi\alpha_p r_p^3 \nabla B^2 - m_p a_p}{6\pi\eta r_p} \quad (4)$$

In Eq. 4, the micro-particles maximum velocity is attained, if the particles acceleration is equivalent to zero. The subsequent equation elucidates the calculation of the maximum velocity:

$$v_m = \frac{2}{9} \frac{\alpha_p r_p^2}{\eta} \nabla B^2 \quad (5)$$

Perfect spherical particles are considered, and F_m represents the force applied in their stimulation. There exists a relationship linking the drag force indicated by F_d in a liquid medium to the particles' velocity, as well as a relation linking the particles' velocity and drag if stable liquid is present. The continuous time model is represented below:

$$m\ddot{x} + C_d * \dot{x} = F_m \quad (6)$$

The drag Stokes of Reynolds continuously designs the drag as low, indicated by $C_d *$, whereas \ddot{x} refers to acceleration. \dot{x} denotes velocity, whereas m denotes the particle mass. Below is an equation exemplifying the micro-particle transfer role.

$$\frac{X(s)}{F_m(s)} = \frac{1}{ms^2 + C_d * s} \tag{7}$$

2.2 PID Controller

With wide usage in industrial applications, the ideal proportional-integral-derivative (PID) controller is a key controller type. It enhances steady state and transient errors performance. Nevertheless, PID controller optimal performance can be compromised if interruptions occur. The most customarily used and broadly applied algorithm in industry is the PID controller. This algorithm, or its slightly varied versions, are employed by most feedback control loops [31]. Three main gains of PID controller can be observed: the integral gain (K_i), the derivative gain (K_d) and the proportional gain (K_p). An action on the error is performed by all of them and is represented in subtracting between the users inserted point and the process measured variable (output). Equation (8) demonstrates the continuous form of the PID controller, incorporating an input error and the controller output, represented as follows:

$$U_{PID} = K_p e(t) + K_I \int_0^t e(t)dt + K_d \frac{d}{dt} e(t) \tag{8}$$

Equation (8) represents the Laplace transform (L.T), while Eq. (9) depicts the PID controller transfer function (T.F). In Fig. 1, an illustration is given of the PID controller standard form in the Laplace transform.

$$C_{PID}(s) = \frac{Y(s)}{E(s)} = K_p + \frac{K_i}{s} + K_d s \tag{9}$$

where the terms K_i , K_p and K_d are used to respectively denote the integral, proportional, and derivative gain.

2.3 Fitness Function Types

Any controller type design necessitates various optimal control parameters. Consequently, distinct parameters need to be computed to minimize the objective function. It should be emphasized that time-dependent errors require multiple functional objectives. Various types of fitness functions can be expressed using the following equations [50–53]:

$$IAE = \int_0^\infty |e(t)|dt \tag{10}$$

$$ISE = \int_0^\infty e^2(t)dt \tag{11}$$

$$ITAE = \int_0^\infty t|e(t)|dt \tag{12}$$

$$ITSE = \int_0^\infty te^2(t)dt \tag{13}$$

$$ISTES = \int_0^\infty [t^2 e(t)]^2 dt \tag{14}$$

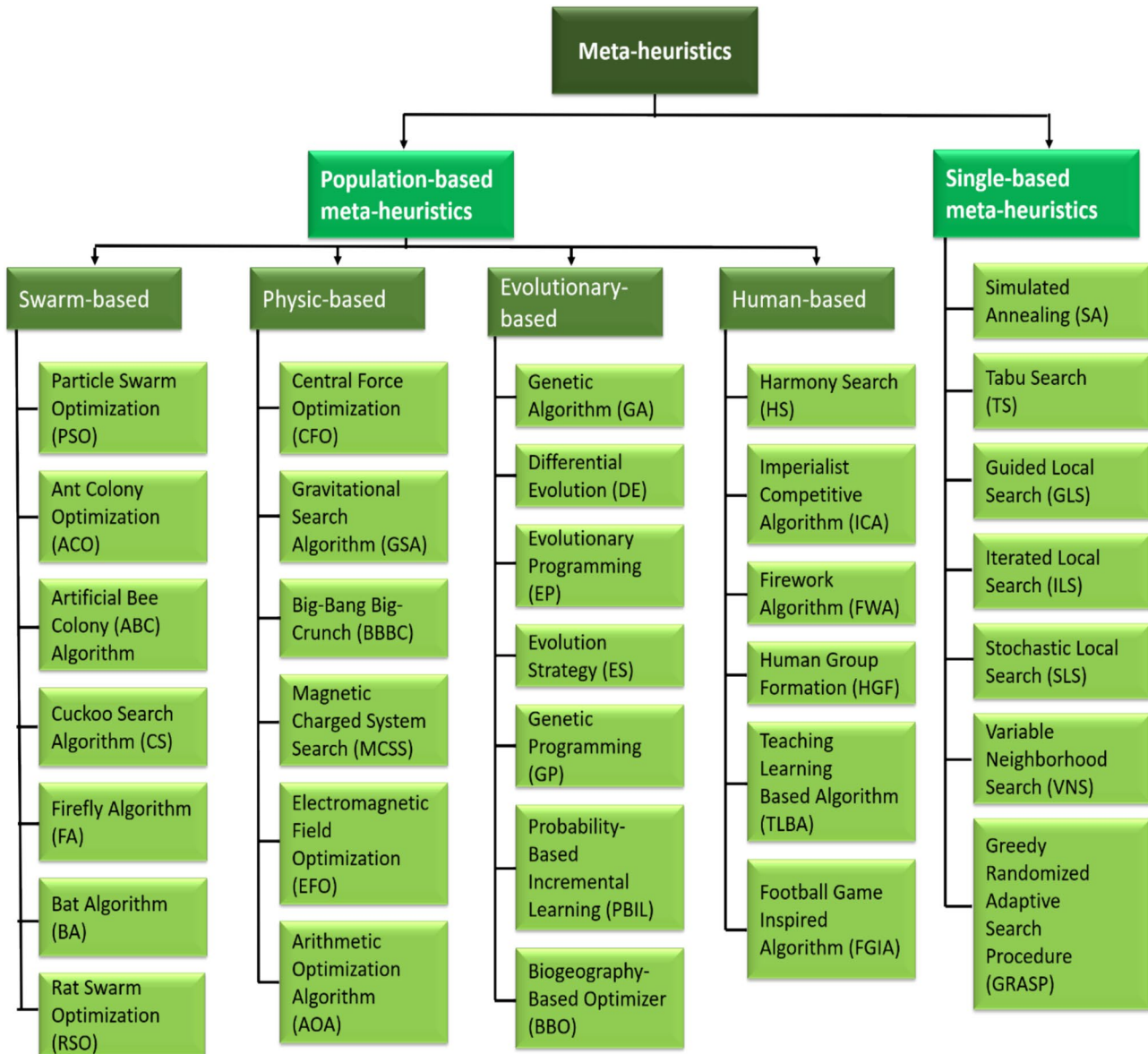


Fig. 1 Meta-heuristic optimization categorization methods

$$ISTSE = \int_0^{\infty} t^2 e^{-t} dt \tag{15}$$

The following guidelines offer formulations for the optimization problem, with minimized objective functions under the conditions below:

$$K_{pmin} < K_p < K_{pmax}$$

$$K_{imin} < K_i < K_{imax}$$

$$K_{dmin} < K_d < K_{dmax}$$

2.4 Optimization Techniques

As discussed in the introduction, it is possible to divide meta-heuristics into four inspiration-based categories. Recombination, selection, and mutation are the three primary processes utilized in evolutionary algorithms, drawing inspiration from natural evolutionary processes. Swarm intelligence algorithms derive their strategies from collective behaviors observed in nature. Physical-based algorithms utilize theories from the multiverse concept for information gathering. Human-based algorithms are influenced by human behaviors and decisions. A commonality among population-based algorithms is their dual-phase approach to searching, involving both exploitation and exploration phases, as indicated in references from the literature. Figure 1 shows some of the most popular algorithms in each category [38–42].

2.4.1 Arithmetic Optimization Algorithm (AOA)

As a novel meta-heuristic optimization technique, the arithmetic optimization algorithm (AOA) [42] draws inspiration from arithmetic operators’ behavior in PC processors or mathematics. It incorporates four primary operations in its calculations, namely division (D), addition (A), multiplication (M), and subtraction (S). The math accelerated optimizer (MOA) function forming the basis of the AOA exploitation and exploration phases is indicated in the equation below:

$$MOA(iter) = Min + iter \left(\frac{Max - Min}{Max_{iter}} \right) \tag{16}$$

Using *iter* and *Max_iter*, respectively, it is possible to define the maximum and current iterations, where *Min* and *Max* indicate the minimum and maximum values’ accelerated functions, respectively.

Exploration phase: Two primary strategies are employed in the exploration phase, namely division (D) and multiplication (M). These strategies aim for discovering the optimum solution. During the exploration phase, update of positions is conducted as represented in this equation:

$$x_{i,j}(iter + 1) = \begin{cases} best(x_j) \div (MOP + \epsilon) * ((ub_j - lb_j)x\mu + lb_j), & r2 > 0.5 \\ best(x_j)x(MOP + \epsilon) * ((ub_j - lb_j)x\mu + lb_j), & otherwise \end{cases} \tag{17}$$

Using $x_{i,j}(iter + 1)$, the *i*th solution’s *j*th position is defined at the current position. $best(x_j)$ represent the best solution realized up till this point at the *j*th position. *U* and *MOP* are represented in the control parameter and the probability math optimizer, respectively. In the equation below, *MOP* is indicated:

$$MOP(iter) = 1 - \left(\frac{iter^{\frac{1}{\alpha}}}{Max_{iter}^{\frac{1}{\alpha}}} \right) \tag{18}$$

α represents the sensitive parameter.

Exploitation phase: Two key operators are essential in this arithmetic optimization algorithm (AOA) phase, namely addition (A) and subtraction (S). Figure 2 illustrates the AOA flowchart employed during this phase. The objective of this phase is to obtain solutions that are both highly optimum and dense.

$$x_{i,j}(iter + 1) = \begin{cases} best(x_j) - (MOP + \epsilon) * ((ub_j - lb_j)x\mu + lb_j), & r3 > 0.5 \\ best(x_j) + (MOP + \epsilon) * ((ub_j - lb_j)x\mu + lb_j), & otherwise \end{cases} \tag{19}$$

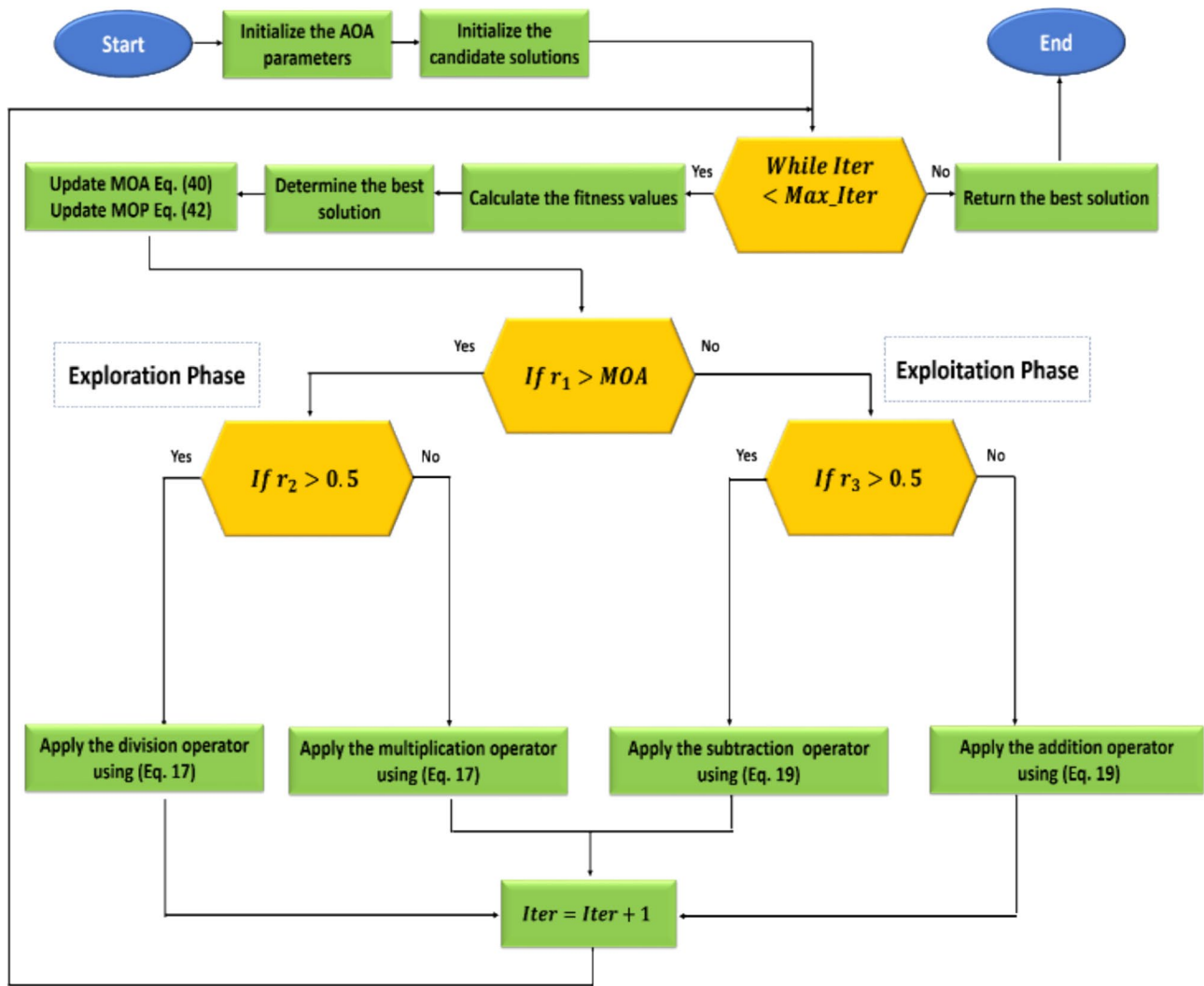


Fig. 2 AOA Flowchart

2.4.2 Rat Swarm Optimization (RSO)

- The rat’s social behavior inspires this algorithm. It is possible to define rats as animal groups comprising males and females. Additionally, rats’ behavior is characterized by aggression, primarily motivating this algorithm. Two key processes dictate the rat’s mathematical model: Chasing and fighting with the prey [49].
- Prey Chasing phase: In this phase, it is possible to consider rats social animals that chase their prey in groups, leaning on particular social agonistic behavior. A mathematical definition of the prey chasing process can be given, depending on the optimum search agent locating the prey’s position. Search agents maintain their focus on their position update, based on the most optimum search agent realized so far. In the equation below, the chasing phase is described below:

$$\bar{P} = A \cdot \bar{P}_i(x) + C \cdot (\bar{P}_r(x) - \bar{P}_i(x)) \tag{20}$$

$$A = R - x \times \left(\frac{R}{Max_{iteration}} \right) \tag{21}$$

where, $x = 0, 1, 2, \dots, Max_{iteration}$

$$C = 2 \cdot rand \tag{22}$$

Within the 1-to-6 range, the parameter C is randomly located, while the 0-to-2 random value is indicated by R. It is noteworthy that it is possible to employ C and A parameters for exploration and exploitation stages or processes.

Fighting with the Prey Phase: The fighting process with the prey is explored in this phase. This process can be represented by a mathematical model defined based on the equation below:

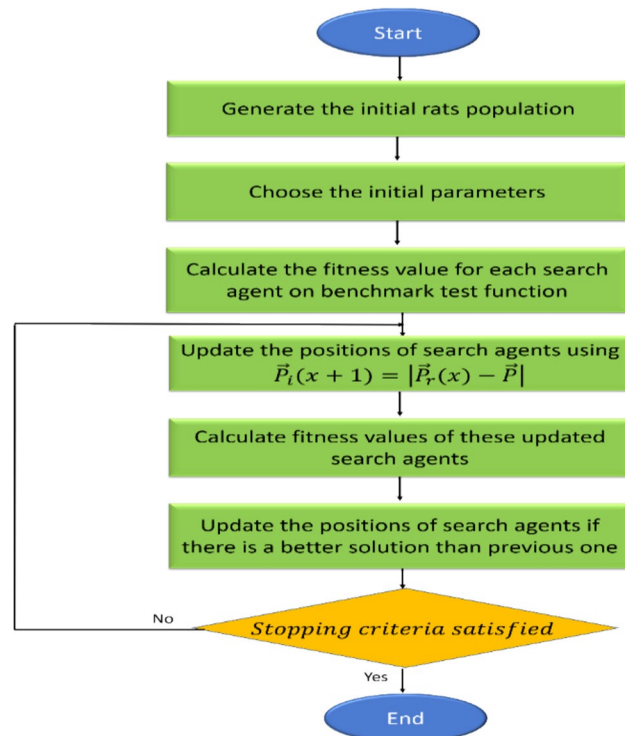
$$\vec{P}_i(x + 1) = \left| \vec{P}_r(x) - \vec{P} \right| \tag{23}$$

The updated rat position based on the next position is indicated by $\vec{P}_i(x + 1)$. Moreover, saving the best position is due to the fact that it is the most optimum solution realized so far, and the update of such position leans on the best search agent. It is noted that it is possible for the rat situated in (A, B) to update the rat position while moving in the direction of prey ((A*, B*). Equations (20) and (23) represent the adjusted parameters for several or various positions, which are achieved by the position currently reached. Thus, for adjusting the exploitation and exploration phases, C and A parameters are employed. RSO flowchart is represented by Fig. 3.

2.4.3 Hybrid AOA-RSO Algorithm (HAOARSO)

In the AOA algorithm, each individual undergoes either the exploration phase (using the Multiplication or Division operator) or the exploitation phase (using the Addition or Sub-traction operator). The RSO algorithm consists

Fig. 3 RSO flowchart



of two steps: chasing the prey and fighting with prey, which are performed by each individual. Individual stages of RSO and AOA algorithms are executed parallelly in the Hybrid AOA-RSO Algorithm. The same population undergoes operations from both the RSO and AOA algorithms. The resulting populations from both algorithms are then combined, and for the next iteration, the best half of the population is selected to be the initial population. Algorithm 1 presents the HAOARSO algorithm pseudocode, while Fig. 4 depicts the HAOARSO flowchart. However, the proposed method involves drawbacks and limitations, including complexity, computational time, and selecting input parameters like constant Parameter Mu, MOP_min, Y, MOP_max, and Alpha control parameter (X) for the hybrid algorithm. To mitigate these issues, the pro-posed HAOAROA algorithm undergoes 30 runs and requires more time to select the optimal parameters for improved performance.

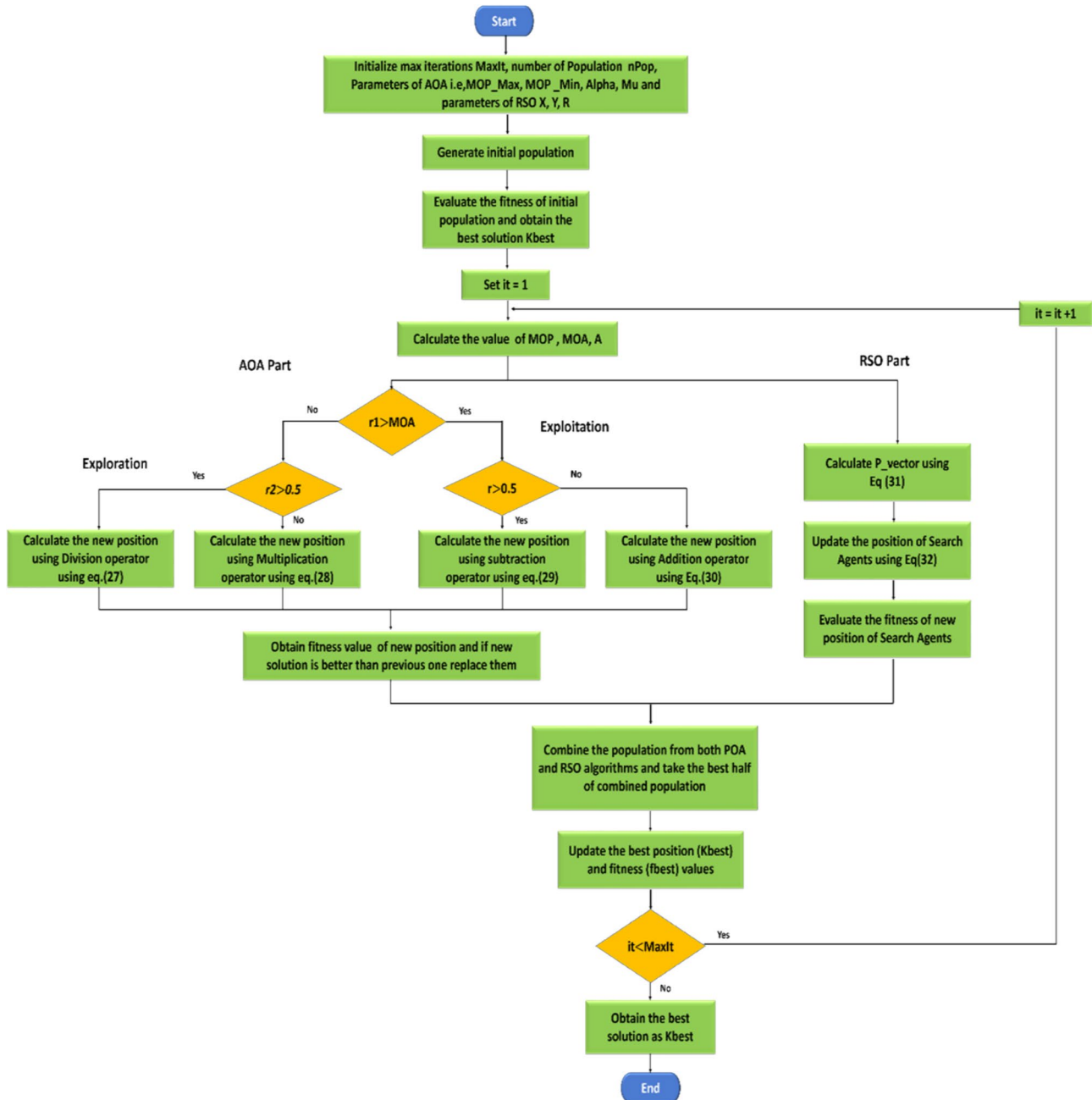


Fig. 4 HAOARSO flowchart

Algorithm 1 Hybrid AOA-RSO (HAOARSO)

Stage1 (Initialization):

Step1: Initialize max iterations MaxIt, number of Population nPop, parameters of AOA i.e, MOP_Max, MOP_Min, Alpha, Mu and parameters of RSO i.e, R

Step2: Initialize the random population K

Step3: Calculate the fitness values of the initial population

Step4: Obtain the best solution Kbest from initial population
Set Iter = 1

Step5:

- Set the AOA and RSO populations both as K, i.e., $K_{aoa} = K_{rso} = K$
- Set the AOA and RSO fitness values both as f i.e., $f_{aoa} = f_{rso} = f$
 - Update the value of MOP using Equation:**
$$MOP = 1 - \left(\frac{it^{1/\alpha}}{MaxIt^{1/\alpha}}\right) \tag{24}$$
- Update the value of MOA using Equation:
$$MOA = MOP_Min + It * \left(\frac{MOP_Max - MOP_Min}{MaxIt}\right) \tag{25}$$
- Update the value of A using equation
$$A = R - R * \left(\frac{It}{MaxIt}\right) \tag{26}$$

Stage2 (AOA Phase):

Step6 (AOA Phase):

- Generate a random number r1
- If $r1 > MOA$ then, Exploration phase
Generate random number r2
 - If $r2 > 0.5$

Apply Division Math operator (\div)
Calculate the positions of solutions (gorillas) using Eq:

$$K_{new_{i,j}} = \frac{K_{Silverback_j}}{(MOP + eps)} * ((K_{max_j} - K_{min_j}) * Mu + K_{min_j}) \tag{27}$$

- Else, Apply Multiply Math operator ($*$)

Calculate positions of solutions (gorillas) using Eq:

$$K_{new_{i,j}} = K_{Silverback_j} * MOP * ((K_{max_j} - K_{min_j}) * Mu + K_{min_j}) \tag{28}$$

- Else, Exploitation phase
 - If $r > 0.5$

Apply Subtraction Math operator ($-$)
Calculate positions of solutions (gorillas) using Eq:

$$K_{new_{i,j}} = K_{Silverback_j} - MOP * ((K_{max_j} - K_{min_j}) * Mu + K_{min_j}) \tag{29}$$

Apply Addition Math operator ($+$)
Calculate the positions of solutions (gorillas) using Eq:

$$K_{new_{i,j}} = K_{Silverback_j} + MOP * ((K_{max_j} - K_{min_j}) * Mu + K_{min_j}) \tag{30}$$

Where, i is the population member and j is the dimension.
Calculate the fitness values of Gorilla

- If New Solutions (K_{new}) are better than previous solutions (K_{aoa}), replace them.
- Update K_{best} as the location of silverback (best location)

Step7 (RSO Phase):

- Search agents update their positions with respect to best search agent obtained so far using Eq:
$$P_vec = A * K_{rso_{i,j}} + abs(C * K_{best_j} - K_{rso_{i,j}}) \tag{31}$$

Where i is the population member and j is the dimension.

- Fighting process of rats with prey, update the position of Search Agents using equation:
$$K_{rso_{i,j}} = K_{best_j} - P_vec \tag{32}$$
- Calculate the fitness values of Search Agents (individuals)
- Combine population of both AOA (K_{aoa}) and RSO (K_{rso}) and take the best half of the population
- Update the best position K_{best} and fitness value f_{best} .

Iter = Iter + 1

- While (Iter < MaxIt)
- Return best solution i.e, K_{best} , and f_{best}

Table 1 The statistical results of the benchmark functions achieved through the application of the hybrid AOARSO algorithm and the original algorithms

Function		AOARSO	AOA	RSO
F1	Best	0	3.1E-91	0
	Mean	3.2E-119	3.98E-26	6.5E-100
	Median	6.3E-169	2.95E-57	0
	Worst	2.8E-118	7.96E-25	1.09E-98
	std	7.2E-119	1.78E-25	2.5E-99
	Rank	1	3	2
F2	Best	0	0	0
	Mean	2.39E-62	7.3E-251	4.41E-54
	Median	0	1.4E-305	0
	Worst	2.92E-61	1.5E-249	8.2E-53
	std	7.37E-62	0	1.83E-53
	Rank	2	1	3
F3	Best	0	3.63E-77	0
	Mean	1.3E-118	0.003975	1.69E-96
	Median	6.7E-169	2.06E-19	0
	Worst	7E-118	0.034951	3.37E-95
	std	2.4E-118	0.008597	7.54E-96
	Rank	1	3	2
F4	Best	0	4.36E-17	0
	Mean	2.39E-55	0.03694	3.16E-16
	Median	1.6E-80	0.043418	0
	Worst	4.78E-54	0.048762	6.31E-15
	std	1.07E-54	0.014199	1.41E-15
	Rank	1	3	2
F5	Best	27.42305	27.75891	28.71037
	Mean	28.1288	28.53532	28.84615
	Median	28.19922	28.62174	28.77426
	Worst	28.44322	28.91855	28.99414
	std	0.262918	0.329828	0.105094
	Rank	1	2	3
F6	Best	0.015043	2.867663	1.170721
	Mean	0.246435	3.429455	2.641882
	Median	0.154218	3.404409	2.875266
	Worst	0.826992	4.148444	3.500434
	std	0.236042	0.282779	0.666583
	Rank	1	3	2
F7	Best	5.07E-06	7.66E-06	3.77E-05
	Mean	4.5E-05	7.69E-05	0.000819
	Median	2.87E-05	4.67E-05	0.000773
	Worst	0.000149	0.000324	0.002059
	std	4.35E-05	7.97E-05	0.000625
	Rank	1	2	3
F8	Best	- 7564.78	- 5931.73	- 7079.6
	Mean	- 6358.25	- 5022.02	- 5796.65
	Median	- 6488.13	- 5046.42	- 6221.09
	Worst	- 5021.78	- 4263.48	- 3001.37
	std	755.8192	375.8013	1163.461
	Rank	1	3	2

Table 1 (continued)

Function		AOARSO	AOA	RSO
F9	Best	0	0	0
	Mean	0	0	0
	Median	0	0	0
	Worst	0	0	0
	std	0	0	0
	Rank	1	1	1
F10	Best	8.88E-16	8.88E-16	8.88E-16
	Mean	8.88E-16	8.88E-16	8.88E-16
	Median	8.88E-16	8.88E-16	8.88E-16
	Worst	8.88E-16	8.88E-16	8.88E-16
	std	0	0	0
	Rank	1	1	1
F11	Best	0	0.013591	0
	Mean	0	0.27439	0
	Median	0	0.253303	0
	Worst	0	0.656816	0
	std	0	0.170068	0
	Rank	1	3	1
F12	Best	0.002808	0.502761	0.096342
	Mean	0.096116	0.597894	0.203111
	Median	0.029584	0.60695	0.207445
	Worst	0.37239	0.665212	0.288589
	std	0.128109	0.040735	0.049709
	Rank	1	3	2
F13	Best	2.86508	2.747742	2.786204
	Mean	2.930237	2.882581	2.883989
	Median	2.966102	2.883638	2.891167
	Worst	2.96621	2.992169	2.921386
	std	0.04322	0.070836	0.031321
	Rank	3	1	2
F14	Best	0.998004	0.998004	0.998004
	Mean	3.558161	9.334357	2.577729
	Worst	12.67051	12.67051	10.76318
	std	2.880125	4.36353	2.137279
	Rank	2	3	1
	F15	Best	0.000314	0.00037
Mean		0.004847	0.015484	0.002032
Median		0.000493	0.013138	0.001121
Worst		0.030834	0.092851	0.020964
std		0.00866	0.02068	0.004471
Rank		2	3	1
F16	Best	- 1.03163	- 1.03163	- 1.03161
	Mean	- 1.03163	- 1.03163	- 1.03138
	Median	- 1.03163	- 1.03163	- 1.03151
	Worst	- 1.03163	- 1.03163	- 1.03024
	std	1.1E-10	1.75E-07	0.000338
	Rank	1	2	3

Table 1 (continued)

Function		AOARSO	AOA	RSO
F17	Best	0.397888	0.3981	0.407392
	Mean	0.397895	0.40942	0.64987
	Median	0.397893	0.409292	0.492055
	Worst	0.397918	0.427246	1.937921
	std	8.33E-06	0.006977	0.374003
	Rank	1	2	3
F18	Best	3	3	3
	Mean	3	4.326596	3.000088
	Median	3	3	3.000015
	Worst	3	29.53193	3.00098
	std	9.9E-10	5.93272	0.000221
	Rank	1	3	2
F19	Best	- 3.86278	- 3.85897	- 3.81955
	Mean	- 3.86265	- 3.85102	- 3.59409
	Median	- 3.86277	- 3.85154	- 3.67927
	Worst	- 3.86112	- 3.83005	- 3.1224
	std	0.000371	0.006144	0.217862
	Rank	1	2	3
F20	Best	- 3.32199	- 3.16924	- 3.03321
	Mean	- 3.26832	- 3.01717	- 2.17138
	Median	- 3.32197	- 3.06691	- 2.0941
	Worst	- 3.20154	- 2.82161	- 1.44767
	std	0.060872	0.11884	0.452557
	Rank	1	2	3
F21	Best	- 10.1518	- 9.39351	- 3.31548
	Mean	- 5.30955	- 4.48857	- 1.09249
	Median	- 5.05474	- 4.37688	- 0.8258
	Worst	- 5.05421	- 2.10831	- 0.40794
	std	1.139747	1.923682	0.741503
	Rank	1	2	3
F22	Best	- 10.4009	- 5.50496	- 2.89211
	Mean	- 5.35275	- 3.63103	- 1.16385
	Median	- 5.08709	- 3.72878	- 0.78527
	Worst	- 5.08632	- 1.65997	- 0.4943
	std	1.188223	1.254071	0.700124
	Rank	1	2	3
F23	Best	- 10.5351	- 7.40726	- 5.58854
	Mean	- 6.20907	- 3.59982	- 1.64654
	Median	- 5.12812	- 2.99909	- 1.13278
	Worst	- 5.12712	- 1.44919	- 0.57624
	std	2.218419	1.700275	1.306267
	Rank	1	2	3
Average Rank	1.217391	2.26087	2.217391	
Final ranking	1	3	2	

Best values are highlighted in bold

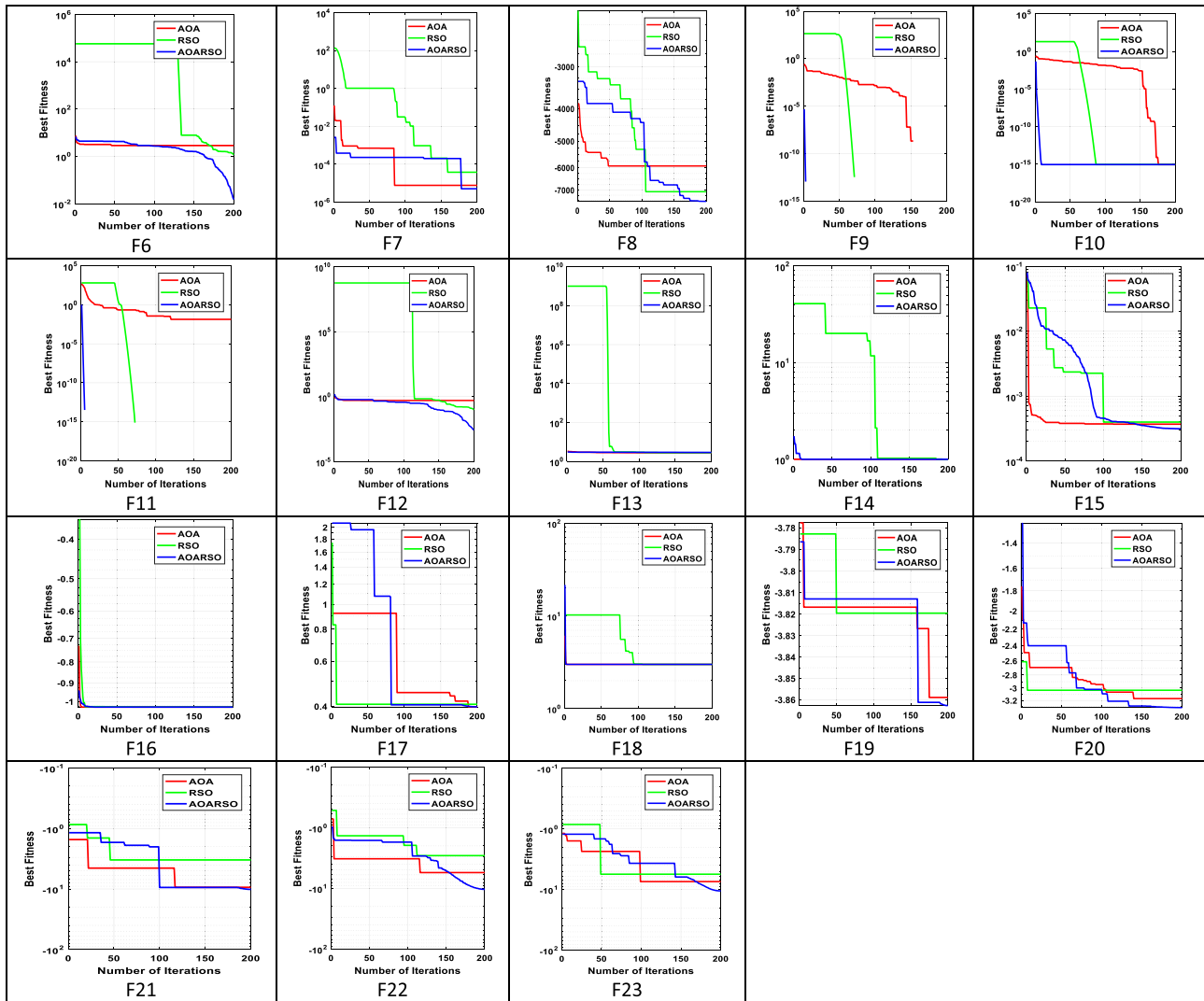


Fig. 5 Convergence curves in 23 benchmark functions examined by the analyzed techniques

3 Performance Analysis of the Proposed HAOARSO

We conducted experiments on 23 benchmark test functions using the hybrid AOARSO technique combined with advanced algorithms. Our aim was to thoroughly evaluate the proposed approach from different angles. We analyzed the exploration and exploitation abilities of the algorithms, as well as their convergence. The presented case studies illustrate the algorithm’s effectiveness in solving complicated problems across various do-mains, highlighting its versatility and adaptability.

3.1 Benchmark Functions

In this subsection, the AOARSO technique’s exceptional performance is demonstrated by experimental results on 23 benchmark functions. MATLAB (R2016a) was employed for experiments to be conducted via a computer featuring 8 GB RAM and Intel(R) Core i5-4210U CPU 2.40 GHz. The objective was comparing the AOARSO

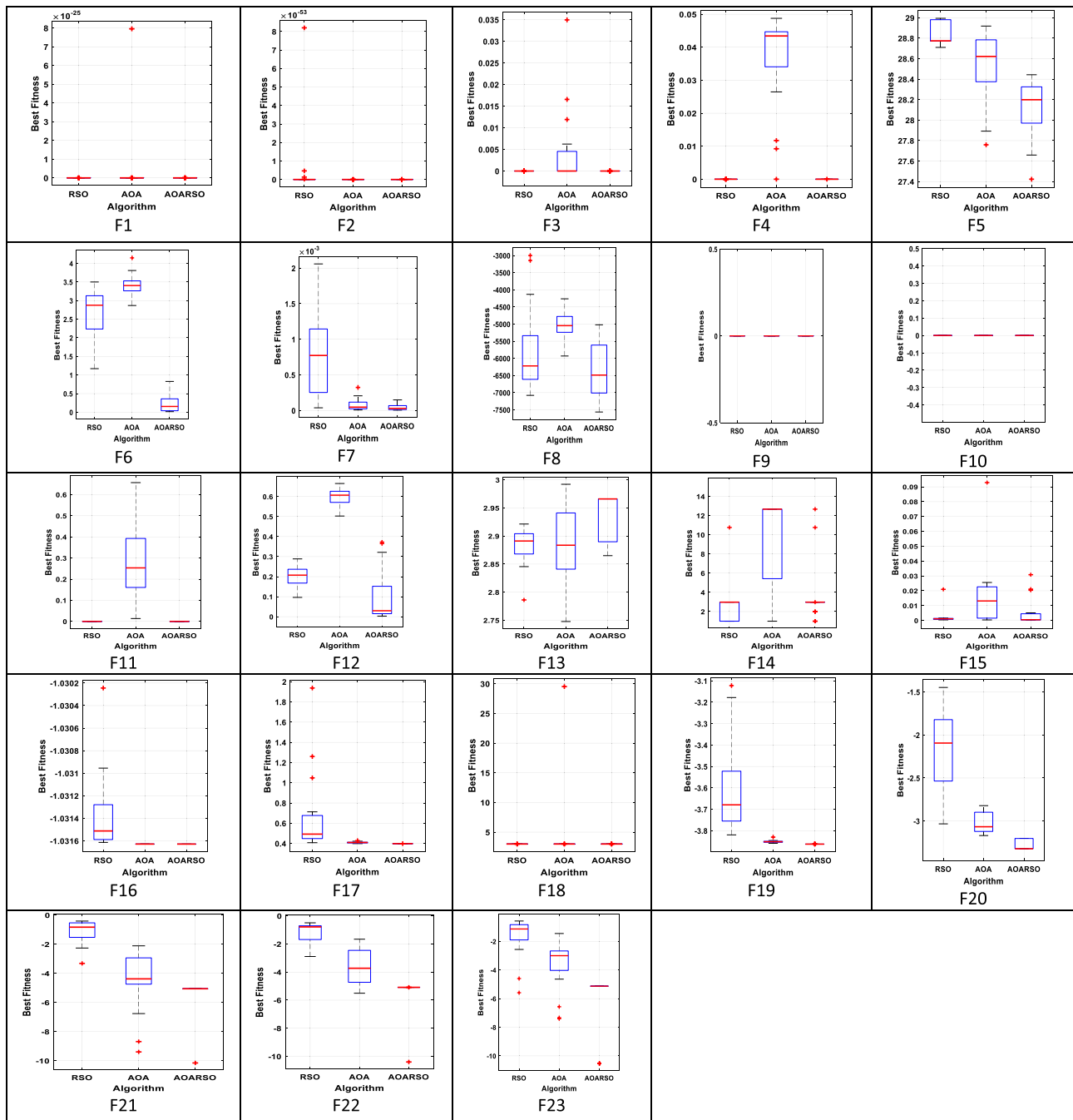


Fig. 6 Examined techniques boxplots for the 23 benchmark functions

algorithm performance with two original metaheuristic techniques, namely AOA and RSO algorithms. To ensure a fair comparison, all techniques were confined to 200 iterations and 50 populations as a maximum.

A comparison of AOA with other optimization techniques, including Particle Swarm Optimization (PSO), Genetic Algorithm (GA), Flower Pollination Algorithm (FPA), Biogeography-based Optimization (BBO), Differential Evolution (DE), Grey Wolf Optimizer (GWO), Firefly Algorithm (FA), Bat Algorithm (BAT), Moth-Flame Optimization (MFO), Cuckoo Search Algorithm (CS), and Gravitational Search Algorithm (GSA) reveals that AOA performs better on various benchmark functions [42]. Similarly, RSO outperforms other methods, such as Grey Wolf Optimizer (GWO), Particle Swarm Optimization (PSO), Spotted Hyena Optimizer (SHO), Multi-Verse

Fig. 7 Micro-robotic system Simulink diagrams of various advanced control techniques

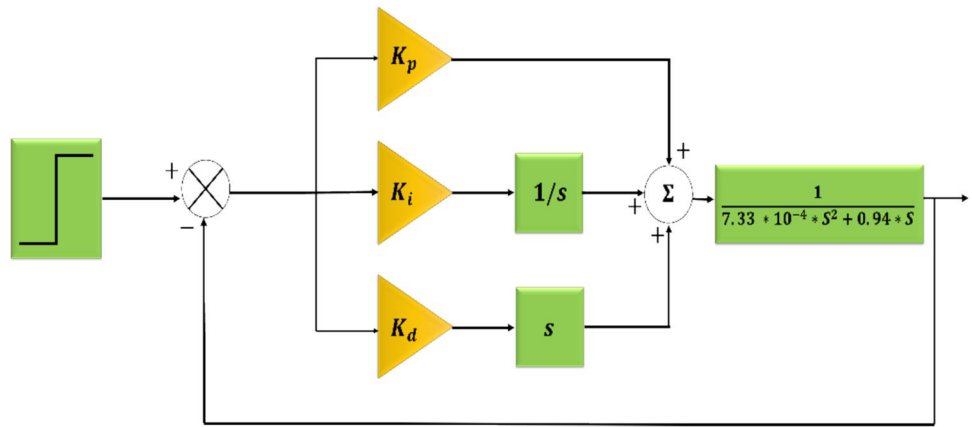


Table 2 The system parameters proposed

Name	Values	Units
Radius (r)	50	μm
Density of water (ρ)	998.2	kg m^{-3}
Dynamic viscosity (ζ)	1	mPa s
Mass (m)	7.33×10^{-10}	Kg
Drag coefficient (cd)	0.94×10^{-6}	N S m^{-1}

Table 3 Input parameters for optimization techniques

Optimization techniques	Parameters	Values
All	Dimension	3
	Min values for K_p, K_i, K_d	[0 0 0]
	Max values for K_p, K_i, K_d	[100 1 1]
	Iter. max	25
	Number of populations	30
HHO	Beta (β) 1.5	
JSO	$\beta=3, C_0=0.5, \gamma=0.1, \eta=4$	
AOA	$f_{\min}=0.07, f_{\max}=0.75, \tau=4.125, a_0=6.25, a_1=100, a_2=0.0005, p_{\min}=0.5, p_{\max}=1.5$	
HAOARSO	MOP_MAX=1, MOP_MIN=0.2, Alpha=5, Mu=0.499, Control parameter (X)=[1, 5], Constant Parameter Y=[0, 2	

Optimizer (MVO), Genetic Algorithm (GA), Moth-Flame Optimization (MFO), Sine Cosine Algorithm (SCA), and Gravitational Search Algorithm (GSA) on well-defined benchmark functions [49]. Since HAOARSO demonstrates superior performance compared to both AOA and RSO on these functions, it can be concluded that HAOARSO outperforms all the previously mentioned optimization techniques.

We evaluated each algorithm’s performance by analyzing the achieved solutions’ standard deviation and mean value, where lower values indicate greater robustness and stability in global optimization. Applying the AOARSO algorithm and five modern techniques to solve the 23 benchmark functions, the statistical results obtained are shown in Table 1, with optimal results highlighted in boldface. Our analysis demonstrates AOARSO algorithm’s

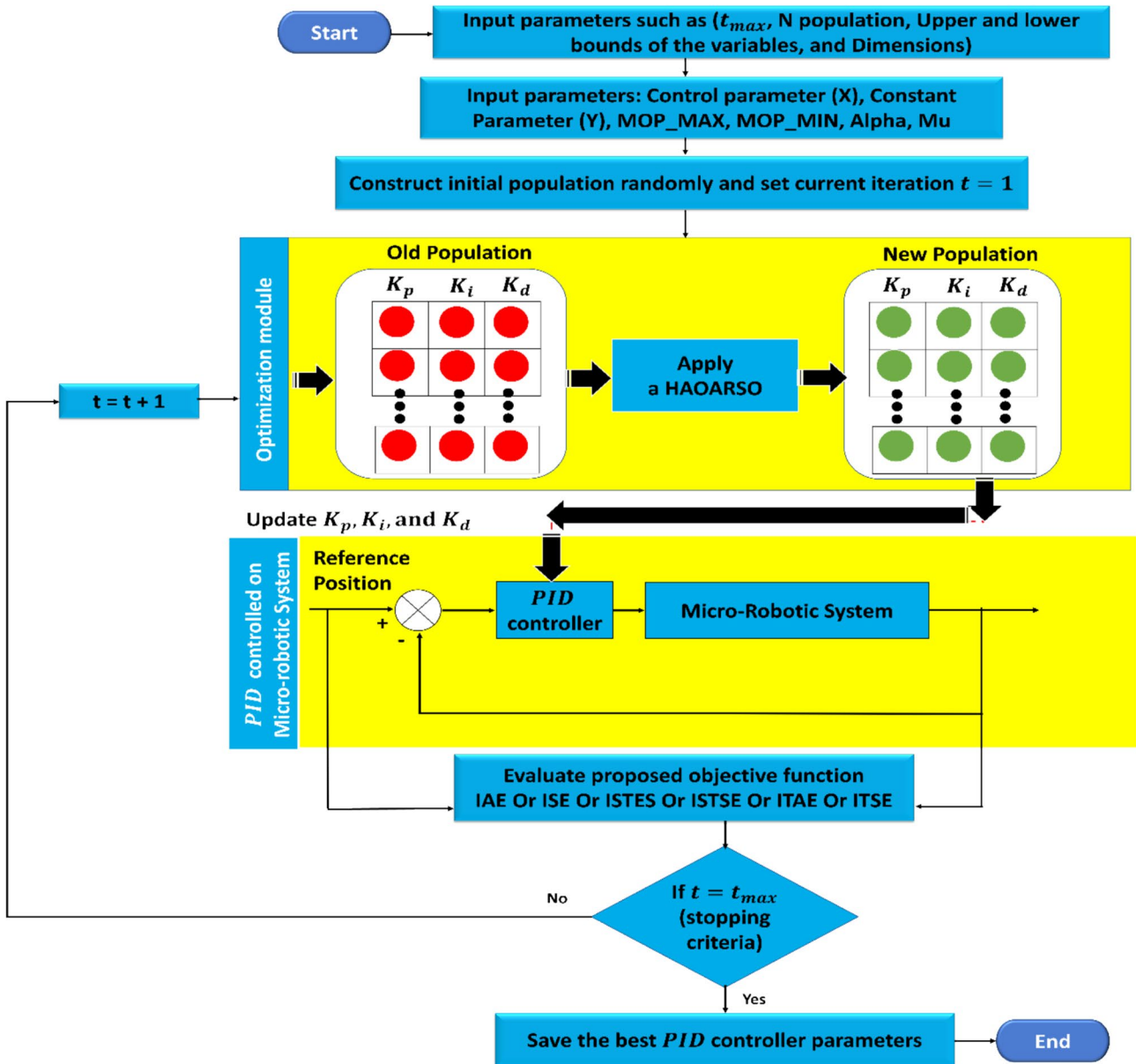


Fig. 8 PID Controller Tuning General Design for Micro-robotic Systems with modern optimization techniques employed

consistent outperformance over other algorithms in average value for most benchmark functions. These results provide compelling evidence for the effectiveness of our approach in identifying global optima across various problems, indicating its potential for real-world applications. Overall, the statistical analysis and visualization of the results strongly support the AOARSO algorithm effectiveness and superiority as a potent tool for optimization globally.

Additionally, each benchmark function convergence curves are illustrated in Fig. 5, providing further evidence on the proposed AOARSO algorithm superior performance in comparison with the original RSO and AOA techniques. AOARSO algorithm’s higher accuracy and faster convergence, when compared to other techniques, are clearly demonstrated by the convergence curves. This observation highlights AOARSO algorithm potential to be a promising solution for addressing complex optimization problems in real-world applications. For the 23 benchmark functions, boxplots of the techniques examined are presented in Fig. 6, emphasizing AOARSO

Table 4 Different optimization techniques’ output in relation to the time response, considering various fitness functions

OA	Fitness	Control parameter			Time response				Best fitness value
		KP	KI	KD	Rise time	Settling time	Peak value	MOS (%)	
JS	IAE	99.988	0.678162	0.016382	6.9390	12.0932	1017.8	1.78	3034.434
	ISE	99.9874	0.973861	0.167866	6.9674	12.0471	1025.4	2.54	1,637,168.1117
	ISTES	99.9832	0.276664	0.066636	6.8934	12.0796	1006.6	0.66	186,946,887.6801
	ISTSE	99.977	0.662382	0.089680	6.9307	12.1012	1017.4	1.74	6,980,630.8896
	ITAE	99.41	0.266732	0.091631	6.8966	12.0837	1006.4	0.64	8980.4867
	ITSE	99.988	0.678162	0.016382	6.9390	12.0932	1017.8	1.78	2,291,771.8468
HHO	IAE	100	0.6314	1	6.9604	12.1362	1016.6	1.66	3042.31
	ISE	100	1	0.9770	6.9863	12.0910	1026.1	2.61	1,638,607.47
	ISTES	100	0.26661	0.3438	6.8967	12.0910	1006.3	0.63	187,684,604.20
	ISTSE	100	0.60484	0	6.9312	12.0948	1015.8	1.58	6,973,321.47
	ITAE	100	0.3187	1	6.9216	12.1229	1007.8	0.78	9017.10
	ITSE	100	1	0	6.9674	12.0471	1026	2.6	2,288,060.00
AOA	IAE	100	0.6664	0	6.9367	12.0922	1017.5	1.75	3033.86
	ISE	100	1	0	6.9674	12.0471	1026	2.6	1,636,466.12
	ISTES	100	0.26866	0	6.8897	12.0746	10,064	0.64	186,687,807.46
	ISTSE	100	0.60416	0	6.9311	12.0948	1015.8	1.58	6,967,332.91
	ITAE	100	0.28996	0	6.8930	12.0777	1007	0.7	8961.89
	ITSE	100	1	0	6.9674	12.0471	1026	2.6	2,288,060.00
HAOARSO	IAE	100	0.6669	0	6.9368	12.0921	1017.5	1.75	3033.838832
	ISE	100	1	0	6.9674	12.0471	1026	2.6	1,636,466.117663
	ISTES	100	0.267227	0	6.8896	12.0744	10,063	0.63	186,686,866.26200
	ISTSE	100	0.604906	0	6.9312	12.0948	1015.8	1.58	6,967,332.193287
	ITAE	100	0.292796	0	6.8934	12.0781	1007.1	0.71	8961.370126
	ITSE	100	1	0	6.9674	12.0471	1026	2.6	2,288,069.998916

Best values are highlighted in bold

algorithm superior performance regarding variance and mean value. Overall, our experiments results confirm that the AOARSO technique is efficient and effective in offering solutions to various optimization problems. While RSO and AOA algorithms also demonstrate robust performance, they may be particularly suitable for specific types of problems.

Based on our study, the AOARSO algorithm exhibited superiority over other algorithms regarding solution quality and convergence speed. Results further highlighted that the AOARSO technique possesses strong exploitation and exploration capabilities, enabling efficient search space exploration and exploitation of promising areas to attain the global optimum. Additionally, our experiments demonstrated the high scalability of the AOARSO algorithm, making it well-suited for addressing complex optimization problems and showcasing its potential across various applications in fields like engineering and finance. Overall, our findings indicate that the AOARSO algorithm holds substantial potential for advancing both research and practical applications in the field of optimization.

4 Simulation

A thorough analysis is presented, in this section, of micro-robotic system performance through employing various advanced control methods. A range of tests is conducted to evaluate and compare the performance of different control approaches. A specific position of 1000 μm employed as the command reference is set to

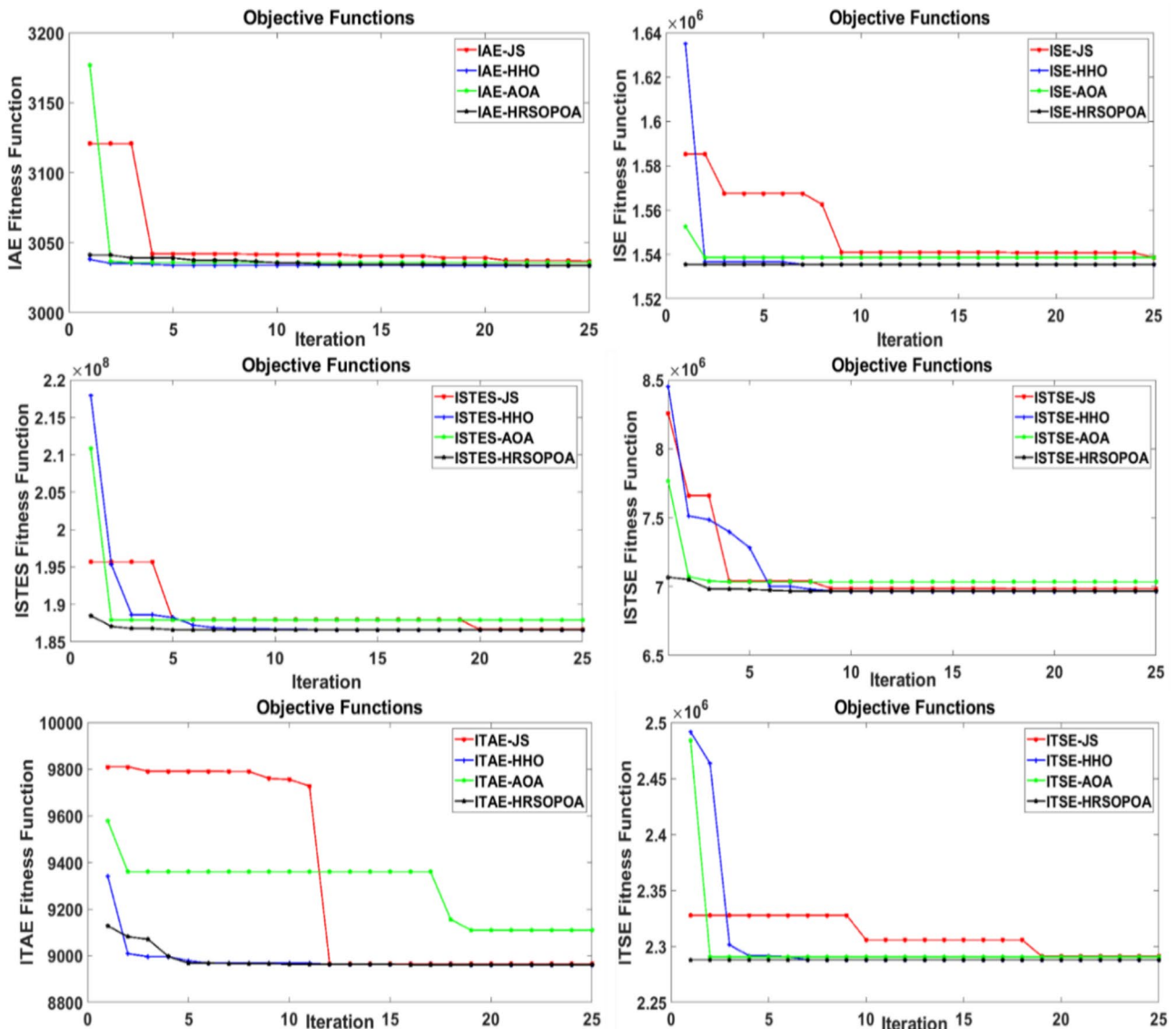


Fig. 9 Convergence curves of various fitness function types for different iteration numbers JS, HHO, AOA, and HAOARSO

ensure consistency. In Fig. 7, illustrating the implementation of various micro-robotic system techniques is displayed in a simulation diagram. Table 2 involves a list of the system parameters proposed, while a summary of the parameters that maintain and control the micro-robotic system position at 1000 μm is given in Table 3.

Figure 8 depicts the overall structure for PID controller tuning through the latest optimization techniques. The process begins with the initialization of control parameters, particularly upper and lower bounds. Next, input parameters are set for the optimization techniques. An application of the optimization techniques is conducted to obtain the PID controller optimal parameter or solution values.

In this scenario, four main advanced optimization techniques are utilized: JSO, HHO, AOA, and HAOARSO. Table 4 presents the output results according to time response, considering numerous fitness functions through simulation. Figure 9 showcases convergence curves for the six fitness functions using JSO, HHO, AOA, and HAOARSO. Notably, HAOARSO demonstrates superior performance compared to JSO, HHO, and AOA, with the

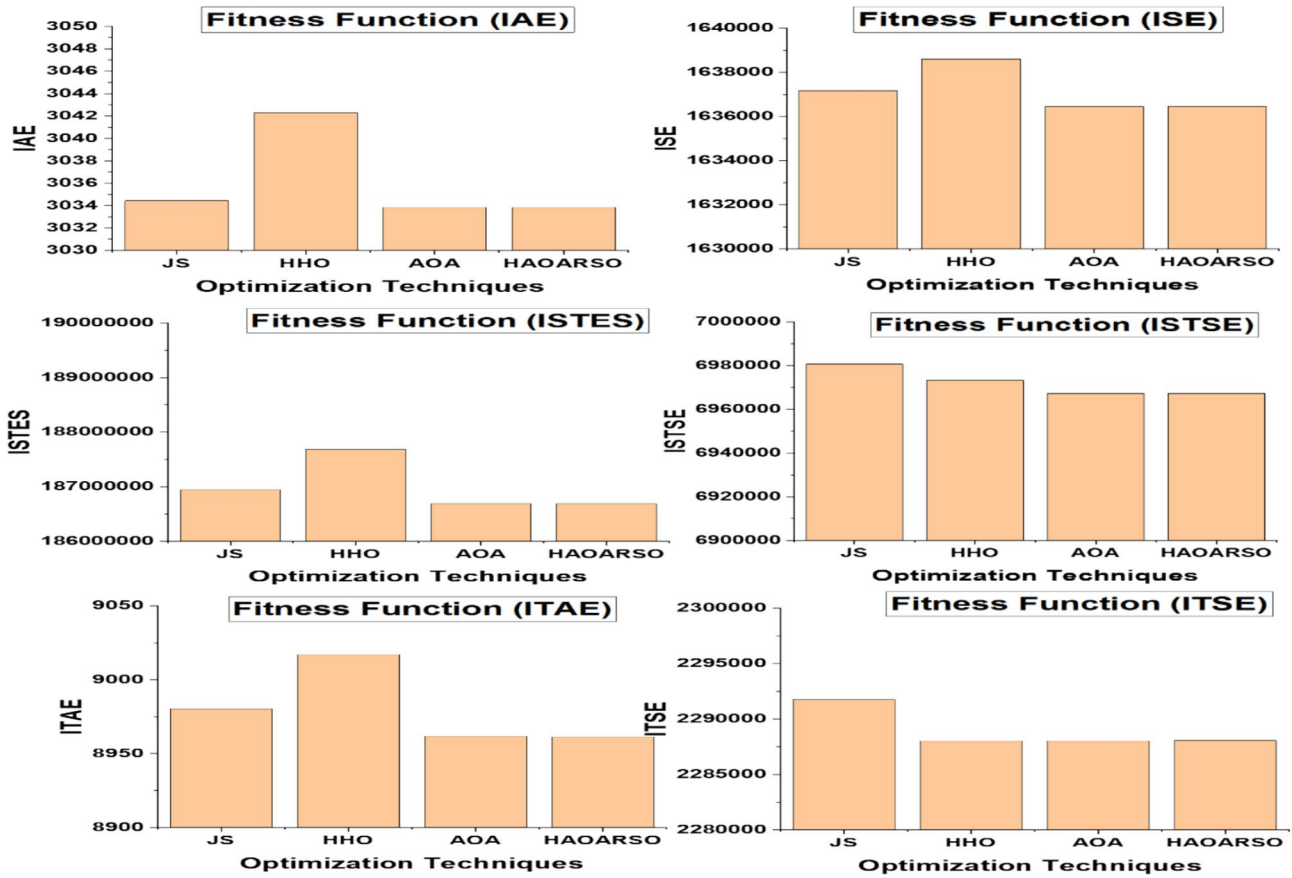


Fig. 10 The bar chart represents the different fitness functions with their best fitness values employing AOA, JS, HHO, and HAOARSO

best fitness function being ISTES. The bar chart in Fig. 10 visually represents the best fitness function employing JSO, HHO, AOA, and HAOARSO. the PID controller.

Table. 5 compares the performance of various optimization techniques across different fitness functions, focusing on frequency response parameters such as gain margin, phase margin, and damping measures. Results indicate that techniques like HHO and AOA achieve slightly better performance in terms of stability and responsiveness for specific fitness functions like ITAE and ISTES.

The Bode diagram in Fig. 11 for the microrobotic system using the HAOARSO technique with a PID controller illustrates its frequency response characteristics, confirming stability and effective control as reflected in consistent phase and gain margins across frequencies. The combined results emphasize the impact of optimization techniques on system control dynamics.

5 Discussion

This section provides a comprehensive comparison of four optimization techniques based on various fitness functions. Parameters considered are best fitness value, settling time, and rising time, which are evaluated using six fitness functions. Six distinct fitness functions (IAE, ITSE, ISTES, ISE, ISTSE, and ITAE) were

Table 5 Different optimization techniques’ output in relation to the frequency response, considering various fitness functions

OA	Fitness	Frequency response					
		GM (dB)	GMF (rad/s)	PM (deg)	PMF (rad/s)	DM (s)	DMF (rad/s)
JS	IAE	0	0	88.7716	0.3192	4.8536	0.3192
	ISE	0	0	88.2693	0.3193	4.8246	0.3193
	ISTES	0	0	89.5011	0.3191	4.8950	0.3191
	ISTSE	0	0	88.8131	0.3192	4.8560	0.3192
	ITAE	0	0	89.5181	0.3173	4.9242	0.3173
	ITSE	0	0	88.7716	0.3192	4.8536	0.3192
HHO	IAE	0	0	89.0354	0.3192	4.8682	0.3192
	ISE	0	0	88.3706	0.3193	4.8302	0.3193
	ISTES	0	0	89.5700	0.3192	4.8981	0.3192
	ISTSE	0	0	88.9003	0.3192	4.8604	0.3192
	ITAE	0	0	89.5965	0.3192	4.8996	0.3192
	ITSE	0	0	88.1923	0.3194	4.8195	0.3194
AOA	IAE	0	0	88.7899	0.3193	4.8541	0.3193
	ISE	0	0	88.1923	0.3194	4.8195	0.3194
	ISTES	0	0	88.9015	0.3192	4.8604	0.3192
	ISTSE	0	0	89.5035	0.3192	4.8944	0.3192
	ITAE	0	0	89.4652	0.3192	4.8923	0.3192
	ITSE	0	0	88.1923	0.3194	4.8195	0.3194
HAOARSO	IAE	0	0	88.7890	0.3193	4.8540	0.3193
	ISE	0	0	88.1923	0.3194	4.8195	0.3194
	ISTES	0	0	89.5060	0.3192	4.8945	0.3192
	ISTSE	0	0	88.9002	0.3192	4.8604	0.3192
	ITAE	0	0	89.4601	0.3192	4.8920	0.3192
	ITSE	0	0	88.1923	0.3194	4.8195	0.3194

Best values are highlighted in bold

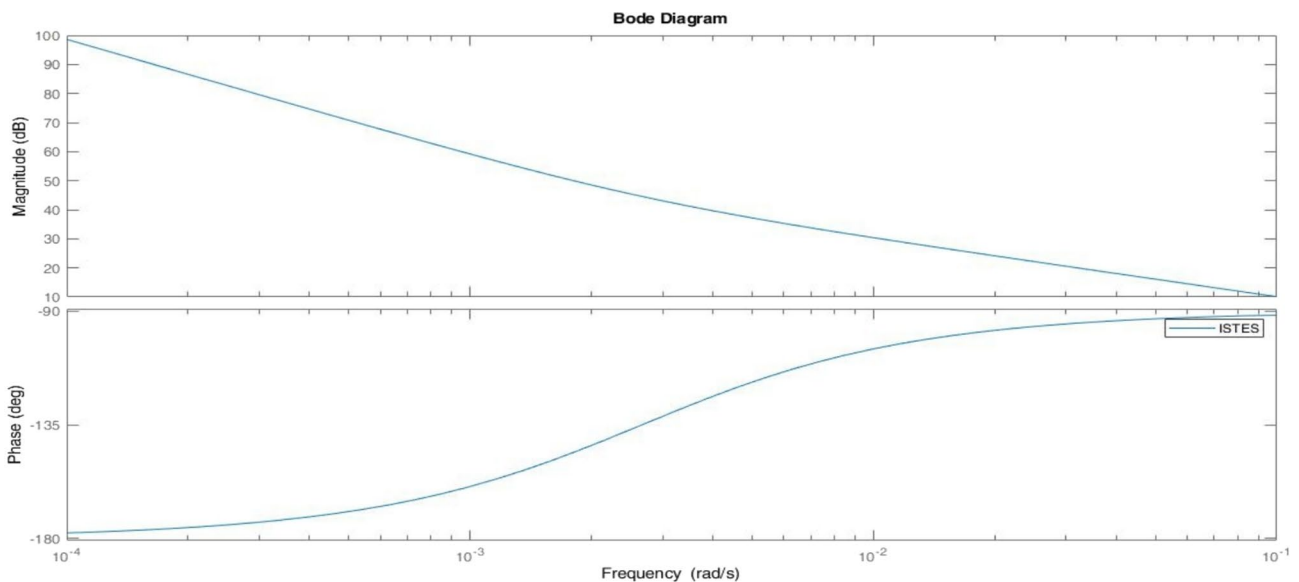


Fig. 11 Microrobotic system Blode Diagram with PID controller-based HAOARSO

employed to evaluate PID controller performance. Each optimization function emphasizes different aspects of system error and response time, offering a comprehensive assessment of the controller's adaptability. MATLAB/Simulink was used to simulate a micro-robotic system under various control strategies (HAOARSO, JSO, HHO, and AOA). The PID parameters were adjusted iteratively to minimize the respective fitness functions, with specific bounds and initializations tailored to each optimization technique. Key metrics, including rise time (T_r), settling time (T_s), and best fitness values, were utilized for comparing the controllers' performance.

HAOARSO algorithm consistently achieved the shortest settling time (T_s) and rise time (T_r) across most simulations, especially when the ISTES fitness function was prioritized. With ISTES as the objective, HAOARSO delivered a T_s of 12.0744 and a T_r of 6.8896, outperforming other algorithms in minimizing transient behavior. ISTES emerged as the most effective fitness function for optimizing the PID controller using HAOARSO. This was evident in its ability to maintain minimal control effort while achieving precision in tracking the desired position. HAOARSO demonstrated superior convergence rates and stability, evidenced by narrower variance and consistently lower mean fitness values in benchmark tests compared to standalone AOA, RSO, and other techniques.

HAOARSO's ability to minimize error metrics and achieve rapid convergence underscores its robustness and suitability for dynamic and precision-critical environments like micro-robotic systems. The hybridization of AOA and RSO effectively leverages their complementary strengths, resulting in a controller design that is not only computationally efficient but also adaptable to diverse system dynamics and constraints. By achieving reduced settling and rise times, HAOARSO enhances the precision and response efficiency of micro-robotic systems. This capability is crucial for applications requiring fine positional control, like targeted drug delivery, or minimally invasive surgical procedures.

The results from previous studies on JSO, HHO, AOA, and HAOARSO are presented in Table 4. Among these techniques, HAOARSO represents the best fitness values, as well as the highest rising and settling time. When simulation results are compared against different control approaches, the superior performance of the HHO technique is demonstrated via best fitness values, settling time, and rising time. Therefore, the HRSOPOA technique proves advantageous for real time prediction in micro-robotics systems.

6 Conclusions

This paper explored four different techniques for optimizing PID controller tuning in micro-robotics systems. The proposed hybrid algorithm, HAOARSO, was successfully implemented to obtain optimal PID parameters, specifically aimed at reducing the ISTES. A comprehensive comparison was conducted among the various algorithms, including AOA, JSO, HHO, and the HAOARSO. Based on analyzing the best fitness values, settling time and rising time, HAOARSO superior performance is manifest in comparison with the other four techniques. Our results confirmed that the application of the proposed HAOARSO outperformed HHO, JSO, and AOA in terms of achieving better outcomes. Therefore, it is recommended to utilize HAOARSO for PID tuning parameters with the ISTES fitness function forming its basis. Additionally, the HRSOPOA technique was found to enhance the efficiency of the system's parameters. In future work, several aspects can be explored to further enhance PID controller tuning for micro-robotics systems. This includes investigating hybrid algorithms combining multiple optimization techniques, exploring alternative controller types such as FOPID or fuzzy PID controllers, conducting real-world experimental validations, optimizing multiple objectives simultaneously, integrating machine learning approaches, and applying the proposed algorithm in different micro-robotics scenarios. These efforts aim to improve the performance, stability, adaptability, and robustness of PID controllers in medical applications and beyond. Future recommendations involve utilizing a hybrid algorithm leaning on two or more algorithms, like Spotted Hyena Optimization (SHO), Honey Badger Algorithm (HBA), etc. For more stable options, it is suggested to use PIDA, FOPID or Fuzzy PID controllers.

Acknowledgements The authors extend their appreciation to King Saud University for funding this work through Researchers Supporting Project number (RSPD2025R697), King Saud University, Riyadh, Saudi Arabia.

Author Contributions Author Contributions: Abdullah Baihan: Methodology; Software; Formal analysis; Funding acquisition; Methodology; Writing—review & editing. Ehab Ghith: Conceptualization; Methodology; Software; Writing—original draft; Writing—review & editing. Harish Garg and Seyedali Mirjalili: Methodology; Software; Writing—original draft; Writing—review & editing. Davut Izci and Mostafa Rashdan: Methodology; Software; Conceptualization; Data curation; Formal analysis; Writing—review & editing. Mohammad Salman, and Kashif Saleem: Methodology; Software; Visualization; Writing—review & editing.

Funding This project was funded by King Saud University through Researchers Supporting Project number (RSPD2025R697), King Saud University, Riyadh, Saudi Arabia.

Data availability No datasets were generated or analysed during the current study.

Declarations

Conflict of interest The authors declare no competing interests.

Ethical approval No studies conducted by any of the authors on animals, rats, or human participants are involved in this article.”

Informed consent All participants involved in the study gave their informed consent.”

Open Access This article is licensed under a Creative Commons Attribution-NonCommercial-NoDerivatives 4.0 International License, which permits any non-commercial use, sharing, distribution and reproduction in any medium or format, as long as you give appropriate credit to the original author(s) and the source, provide a link to the Creative Commons licence, and indicate if you modified the licensed material. You do not have permission under this licence to share adapted material derived from this article or parts of it. The images or other third party material in this article are included in the article’s Creative Commons licence, unless indicated otherwise in a credit line to the material. If material is not included in the article’s Creative Commons licence and your intended use is not permitted by statutory regulation or exceeds the permitted use, you will need to obtain permission directly from the copyright holder. To view a copy of this licence, visit <http://creativecommons.org/licenses/by-nc-nd/4.0/>.

References

1. Pankhurst, Q.A., Connolly, J., Jones, S.K., Dobson, J.: Applications of magnetic nanoparticles in biomedicine. *J. Phys. D Appl. Phys.* **36**(13), R167 (2003)
2. Nelson, B.J., Kaliakatsos, I.K., Abbott, J.J.: Microrobots for minimally invasive medicine. *Annu. Rev. Biomed. Eng.* **12**, 55–85 (2010)
3. Sinha, R., Kim, G.J., Nie, S., Shin, D.M.: Nanotechnology in cancer therapeutics: bioconjugated nanoparticles for drug delivery. *Mol. Cancer Ther.* **5**(8), 1909–1917 (2006)
4. Martel, S., Felfoul, O., Mathieu, J.B., Chanu, A., Tamaz, S., Mohammadi, M., Tabatabaei, N.: MRI-based medical nanorobotic platform for the control of magnetic nanoparticles and flagellated bacteria for target interventions in human capillaries. *Int J Robotics Res* **28**(9), 1169–1182 (2009)
5. Khalil, I. S., Gomaa, I. E., Abdel-Kader, R. M., & Misra, S. (2016). Magnetic-Based contact and non-contact manipulation of cell mockups and MCF-7 human breast cancer cells. *Smart Drug Delivery System*, 219–235.
6. Belharet, K., Folio, D., Ferreira, A.: Simulation and planning of a magnetically actuated microrobot navigating in the arteries. *IEEE Trans. Biomed. Eng.* **60**(4), 994–1001 (2012)
7. Wang, J., Gao, W.: Nano/microscale motors: biomedical opportunities and challenges. *ACS Nano* **6**(7), 5745–5751 (2012)
8. Youakim, K., Ehab, M., Hatem, O., Misra, S., & Khalil, I. S. (2015). Paramagnetic microparticles sliding on a surface: characterization and closed-loop motion control. In 2015 IEEE International Conference on Robotics and Automation (ICRA). IEEE, pp. 4068–4073
9. Shevkoplyas, S.S., Siegel, A.C., Westervelt, R.M., Prentiss, M.G., Whitesides, G.M.: The force acting on a superparamagnetic bead due to an applied magnetic field. *Lab Chip* **7**(10), 1294–1302 (2007)

10. Weizenecker, J., Gleich, B., Rahmer, J., Dahnke, H., Borgert, J.: Three-dimensional real-time in vivo magnetic particle imaging. *Phys. Med. Biol.* **54**(5), L1 (2009)
11. Lübbe, A.S., Bergemann, C., Brock, J., McClure, D.G.: Physiological aspects in magnetic drug-targeting. *J. Magn. Magn. Mater.* **194**(1–3), 149–155 (1999)
12. Rudge, S.R., Kurtz, T.L., Vessely, C.R., Catterall, L.G., Williamson, D.L.: Preparation, characterization, and performance of magnetic iron–carbon composite microparticles for chemotherapy. *Biomaterials* **21**(14), 1411–1420 (2000)
13. Alexiou, C., Arnold, W., Klein, R.J., Parak, F.G., Hulin, P., Bergemann, C., Lubbe, A.S.: Locoregional cancer treatment with magnetic drug targeting. *Cancer Res.* **60**(23), 6641–6648 (2000)
14. Sanchez, S., Solovev, A.A., Harazim, S.M., Schmidt, O.G.: Microbots swimming in the flowing streams of microfluidic channels. *J. Am. Chem. Soc.* **133**(4), 701–703 (2011)
15. Khalil, I. S., Pichel, M. P., Reefman, B. A., Sukas, O. S., Abelman, L., & Misra, S. (2013). Control of magnetotactic bacterium in a micro-fabricated maze. In 2013 IEEE International Conference on Robotics and Automation. IEEE, pp. 5508–5513
16. Khalil, I.S., Magdanz, V., Sanchez, S., Schmidt, O.G., Misra, S.: Precise localization and control of catalytic Janus micromotors using weak magnetic fields. *Int. J. Adv. Rob. Syst.* **12**(1), 2 (2015)
17. Belharet, K., Folio, D., & Ferreira, A. (2012). Control of a magnetic microrobot navigating in microfluidic arterial bifurcations through pulsatile and viscous flow. In 2012 IEEE/RSJ International Conference on Intelligent Robots and Systems. IEEE, pp. 2559–2564
18. Khalil, I.S., Magdanz, V., Sanchez, S., Schmidt, O.G., Misra, S.: The control of self-propelled microjets inside a microchannel with time-varying flow rates. *IEEE Trans. Rob.* **30**(1), 49–58 (2013)
19. Nacev, A., Beni, C., Bruno, O., Shapiro, B.: Magnetic nanoparticle transport within flowing blood and into surrounding tissue. *Nanomedicine* **5**(9), 1459–1466 (2010)
20. Khalil, I. S., Metz, R. M., Reefman, B. A., & Misra, S. (2013). Magnetic-Based minimum input motion control of paramagnetic microparticles in three-dimensional space. In 2013 IEEE/RSJ International Conference on Intelligent Robots and Systems. IEEE, pp. 2053–2058
21. Keuning, J. D., de Vries, J., Abelman, L., & Misra, S. (2011). Image-based magnetic control of paramagnetic microparticles in water. In 2011 IEEE/RSJ International Conference on Intelligent Robots and Systems. IEEE, pp. 421–426
22. Farag, R., Badawy, I., Magdy, F., Mahmoud, Z., & Sallam, M. (2020). Real-time trajectory control of potential drug carrier using pantograph “experimental study”. In International Conference on Advanced Intelligent Systems and Informatics. Springer, Cham, pp. 305–313
23. Ghith, E. S., & Tolba, F. A. A. (2022). Real-Time Implementation of Tuning PID Controller Based on Whale Optimization Algorithm for Micro-robotics System. In 2022 14th International Conference on Computer and Automation Engineering (ICCAE). IEEE, pp. 103–109
24. Ghith, E. S., Tolba, F. A., & Hammad, S. A. (2022). Real-Time Implementation of Tuning PID Controller Based on Sine Cosine Algorithm for Micro-robotics System. In International Conference on Digital Technologies and Applications. Springer, Cham, pp. 801–811
25. Ghith, E.S., Tolba, F.A.A.: Real-time implementation of an enhanced proportional-integral-derivative controller based on a sparrow search algorithm for micro-robotics system. *IAES Int. J. Artif. Intell.* **11**(4), 1395–1404 (2022)
26. Ghith, E. S., & Tolba, F. A. A. (2022, May). Real-Time Implementation of an Enhanced PID CONTROLLER based on Marine Predator Algorithm (MPA) for Micro-robotics System. In 2022 3rd International Conference on Artificial Intelligence, Robotics and Control (AIRC). IEEE, pp. 40–45
27. Ghith, E.S., Tolba, F.A.A.: Real-time implementation of an enhanced pid controller based on ant lion optimizer for micro-robotics system. *Math. Modelling Eng. Probl.* **9**(4), 1113–1122 (2022)
28. Ghith, E.S., Tolba, F.A.A.: Tuning PID controllers based on hybrid arithmetic optimization algorithm and artificial gorilla troop optimization for micro-robotics systems. *IEEE Access* **11**, 27138–27154 (2023)
29. Ghith, E.S., Tolba, F.A.: Design and optimization of pid controller using various algorithms for micro-robotics system. *J. Robot. Control. JRC* **3**, 244–256 (2022)
30. Ghith, E.S., Tolba, F.A.A.: LabVIEW implementation of tuning PID controller using advanced control optimization techniques for micro-robotics system. *Int. J. Mech. Eng. Robot. Res.* **11**, 653–661 (2022)
31. Astrom, K.J., Hagglund, T., Controllers, P.I.D.: Theory, design, and tuning, 2nd edn. Instrument Society of America, Research Triangle Park, NC, USA (1995)
32. T. Mansour, PID Controller Implementation and Tuning. Rijeka, Croatia: InTech, 2011.
33. Ogata, K.: Modern control engineering. Prentice-Hall, Upper Saddle River, NJ, USA (2010)
34. Hägglund, T., Åström, K.J.: ‘Revisiting the Ziegler-Nichols tuning rules for pi control.’ *Asian J. Control* **4**(4), 364–380 (2008)
35. Tan, W., Liu, J., Chen, T., Marquez, H.J.: ‘Comparison of some well-known PID tuning formulas.’ *Comput. Chem. Eng.* **30**(9), 1416–1423 (2006)
36. Visioli, A.: ‘Research trends for PID controllers.’ *Acta Polytech.* **52**(5), 144–150 (2012)

37. Valério, D., da Costa, J.S.: 'Tuning of fractional PID controllers with Ziegler–Nichols-type rules.' *Signal Process.* **86**(10), 2771–2784 (2006)
38. Maghade, D.K., Patre, B.M.: Pole placement by PID controllers to achieve time domain specifications for TITO systems. *Trans. Inst. Meas. Control.* **36**, 506–522 (2014)
39. Bingul, Z., Karahan, O.: Comparison of PID and FOPID controllers tuned by PSO and ABC algorithms for unstable and integrating systems with time delay. *Optim. Control. Appl. Methods* **39**, 1431–1450 (2018)
40. Singh, N., Hamid, Y., Juneja, S., Srivastava, G., Dhiman, G., Gadekallu, T.R., Shah, M.A.: Load balancing and service discovery using Docker Swarm for microservice based big data applications. *J. Cloud Comput.* **12**, 1–9 (2023)
41. Nayak, J., Swapnarekha, H., Naik, B., Dhiman, G., Vimal, S.: 25 years of particle swarm optimization: flourishing voyage of two decades. *Arch. Comput. Methods Eng.* (2022). <https://doi.org/10.1007/s11831-022-09849-x>
42. Abualigah, L., Diabat, A., Mirjalili, S., Abd Elaziz, M., Gand Omi, A.H.: The arithmetic optimization algorithm. *Comput. Methods Appl. Mech. Eng.* **376**, 113609 (2021)
43. Izci, D., Ekinici, S., Hussien, A.G.: Effective PID controller design using a novel hybrid algorithm for high order systems. *PLoS ONE* **18**(5), e0286060 (2023)
44. Izci, D., & Ekinici, S. (2022, February). A novel hybrid ASO-NM algorithm and its application to automobile cruise control system. In *Proceedings of 2nd International Conference on Artificial Intelligence: Advances and Applications: ICAIAA 2021*. Singapore: Springer Nature Singapore, pp. 333–343
45. Eker, E., Kayri, M., Ekinici, S., Izci, D.: A new fusion of ASO with SA algorithm and its applications to MLP training and DC motor speed control. *Arab. J. Sci. Eng.* **46**, 3889–3911 (2021)
46. Izci, D., Ekinici, S., Kayri, M., Eker, E.: A novel improved arithmetic optimization algorithm for optimal design of PID controlled and Bode's ideal transfer function based automobile cruise control system. *Evol. Syst.* **13**(3), 453–468 (2022)
47. Izci, D., Hekimoglu, B., Ekinici, S.: A new artificial ecosystem-based optimization integrated with Nelder-Mead method for PID controller design of buck converter. *Alexandria Eng J* **61**, 2030–2044 (2022)
48. Izci, D., Ekinici, S.: A novel-enhanced metaheuristic algorithm for FOPID-controlled and Bode's ideal transfer function-based buck converter system. *Trans. Inst. Meas. Control.* **45**(10), 1854–1872 (2023)
49. Dhiman, G., Garg, M., Nagar, A., Kumar, V., Dehghani, M.: A novel algorithm for global optimization: rat swarm optimizer. *J. Ambient. Intell. Humaniz. Comput.* **12**(8), 8457–8482 (2021)
50. Sallam, Mohamed; Saif, I.; Saeed, Z.; Fanni, M. Lyapunov-based control of a teleoperation system in the presence of time delay. In: *International Conference on Advanced Intelligent Systems and Informatics*; Springer: Cham, Switzerland, 2020; pp. 759–768.
51. Aribowo, W., Ghith, E.S., Rahmadian, R., Widyartono, M., Wardani, A.L., Prapanca, A.: Sand cat swarm optimization for controlling PID in DC motor. *TELKOMNIKA (Telecommun. Comput. Electron. Control)* **22**(2), 462–470 (2024)
52. Abushanab, A. M., Hasanien, H. M., & Sharkawy, R. M. (2024). Frequency Control of Interconnected Power System Using Dandelion Optimization Algorithm. In *2024 6th International Youth Conference on Radio Electronics, Electrical and Power Engineering (REEPE)*. IEEE, pp. 1–7
53. Abushanab, A. M., Hasanien, H. M., & Sharkawy, R. M. (2024). Frequency Control of Interconnected Power System Utilizing Novel Optimization Approaches. In: *2024 FORTEI-International Conference on Electrical Engineering (FORTEI-ICEE)*. IEEE., pp. 24–29

Publisher's Note Springer Nature remains neutral with regard to jurisdictional claims in published maps and institutional affiliations.

Authors and Affiliations

Abdullah Baihan¹ · Ehab Ghith² · Harish Garg³ · Seyedali Mirjalili⁴ · Davut Izci^{5,8,9} · Mostafa Rashdan⁶ · Mohammad Salman⁶ · Kashif Saleem⁷

✉ Ehab Ghith
drehabghith1978@gmail.com

Abdullah Baihan
aalbaihan@ksu.edu.sa

Harish Garg
harish.garg@thapar.edu

Syedali Mirjalili
ali.mirjalili@gmail.com

Davut Izci
davutizci@gmail.com; davutizci@uludag.edu.tr

Mostafa Rashdan
mostafa.rashdan@aum.edu.kw

Mohammad Salman
mohammad.salman@aum.edu.kw

Kashif Saleem
Ksaleem@ksu.edu.sa

- ¹ Computer Science Department, Community College, King Saud University, 11437 Riyadh, Saudi Arabia
- ² Department of Mechatronics, Faculty of Engineering, Ain Shams University, Cairo 11566, Egypt
- ³ Department of Mathematics, Thapar Institute of Engineering & Technology (Deemed University), Patiala, Punjab 147004, India
- ⁴ Centre for Artificial Intelligence Research and Optimisation, Torrens University Australia, Brisbane, Australia
- ⁵ Department of Electrical and Electronics Engineering, Bursa Uludag University, 16059 Bursa, Turkey
- ⁶ College of Engineering and Technology, American University of the Middle East, 54200 Egaila, Kuwait
- ⁷ Department of Computer Science & Engineering, College of Applied Studies & Community Service, King Saud University, 11362 Riyadh, Saudi Arabia
- ⁸ Applied Science Research Center, Applied Science Private University, 11931 Amman, Jordan
- ⁹ Jadara University Research Center, Jadara University, Irbid, Jordan